ACS APPLIED MATERIALS & INTERFACES

Research Article

www.acsami.org

Carbon-Based Nanoreporters Designed for Subsurface Hydrogen Sulfide Detection

Chih-Chau Hwang,[#,†] Gedeng Ruan,[#,†] Lu Wang,[#,‡] Haiyan Zheng,[†] Errol L. G. Samuel,[†] Changsheng Xiang,[†] Wei Lu,[†] William Kasper,[†] Kewei Huang,[†] Zhiwei Peng,[†] Zachary Schaefer,[§] Amy T. Kan,[‡] Angel A. Martí,[†,∥] Michael S. Wong,[*,†,§] Mason B. Tomson,[*,‡] and James M. Tour[*,†,∥,⊥]

[†]Department of Chemistry, [‡]Department of Civil and Environmental Engineering, [§]Department of Chemical and Biomolecular Engineering, [∥]The Richard E. Smalley Institute for Nanoscale Science and Technology, and [⊥]The Department of Materials Science and NanoEngineering, Rice University, 6100 Main Street, Houston, Texas 77005, United States

Supporting Information

ABSTRACT: Polyvinyl alcohol functionalized carbon black with H_2S-sensor moieties can be pumped through oil and water in porous rock and the H_2S content can be determined based on the fluorescent enhancement of the H_2S-sensor addends.

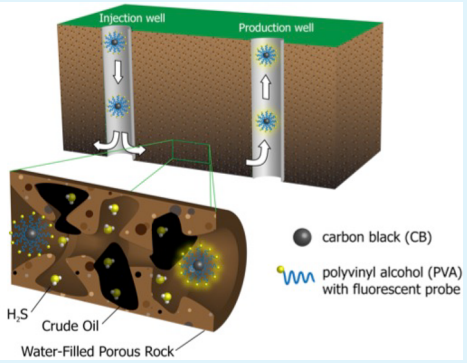

KEYWORDS: *nanoparticle, H_2S detection, fluorescent enhancement, carbon black, breakthrough study, polyvinyl alcohol (PVA)*

INTRODUCTION

Hydrogen sulfide is considered a broad spectrum poison that can adversely affect several different systems in the human body.[1] The toxicity of H_2S is even stronger than that of hydrogen cyanide in terms of the half maximal inhibitory concentration (IC_{50}).[2] It is worth noting that the human nose quickly becomes desensitized to H_2S, leading to an inability to detect higher concentrations of H_2S that could cause rapid death. After exposure to nonlethal levels of H_2S, humans may suffer sore throats, shortness of breath, and dizziness.[3] Recent studies also observed that H_2S is a biologically important signaling molecule in various tissues and processes including pain and inflammation;[4] therefore, chemists have synthesized a series of fluorescent probes for H_2S detection. We capitalize upon those probes here for downhole detection of H_2S in oilfields.

The presence of H_2S has a significant impact on the quality of crude oil in which it is found. Decayed organic material (kerogen) that is found in sedimentary rock formations can have high sulfur content. During thermal decomposition of the kerogen into crude oil or natural gas, H_2S can be one of the products.[5] As a result, crude oil and natural gas inherently contain varying amounts of H_2S, depending on the original sulfur content of the kerogen.[5] Crude oil is classified as "sour" when it contains a total sulfur content greater than 0.5%.[6] Among these sulfur species, H_2S is the one of main impurities in sour crude. The sour crude is toxic and corrosive to the materials of construction in pipelines and other holding and transportation vessels. The sulfur impurities must be reduced to varying levels by additional refining steps. The reduction levels depend upon regulations and the targeted product slate before being refined into distilled products. These extra steps normally result in higher-priced fuel products than those made from "sweet", or low-sulfur content, crude oil.[7] Today's oil refineries are facing a problem as they have limited capacities to process the increasing amounts of sour crude being produced, especially regarding the processing of the heavier sour grades of crude oil.[7] The amount of sulfur in a sample of crude depends on where it was found. If the concentration of the sulfur species in the subsurface could be accurately monitored, then geologists might be able to evaluate the quality of the crude before large scale extraction ensues.

Recently, nanomaterials have been studied for transport through porous media[8−15] and they are expected to have significantly different transport behaviors than those of traditional polymers. For instance, injecting nanoparticles (NPs) through simulated downhole porous media provides an innovative approach for subsurface oil detection and enhanced oil recovery.[11,12,16,17] Among these techniques, however, the design of a NP with an acceptable terrestrial

Received: February 14, 2014
Accepted: April 15, 2014
Published: April 15, 2014

   dx.doi.org/10.1021/am5009584 | ACS Appl. Mater. Interfaces 2014, 6, 7652−7658

transport efficiency is considered a formidable challenge because the NPs are prone to aggregation in the downhole environment of high temperature and high salinity, which could greatly restrain NP transport, decreasing the breakthrough efficiency.

In recent work, we developed a carbon black (CB)-based NP with high mobility and thermal stability that survives high temperature and high salinity conditions so that it could efficiently transport the cargo molecules through simulated downhole formations, effectively conducting subsurface exploration as a nanoreporter.[17] These results have implications in downhole oil detection, enhanced oil recovery and environmental remediation of contaminated land.

Here, we synthesized a newly designed nanoreporter by attaching H_2S-sensitive probe molecules onto the NPs; these functionalized NPs have the potential to detect H_2S downhole with assessment immediately upon return to the surface. Based on prior work, the functionalized NPs should have high mobility and stability in the downhole environment. Figure 1 is

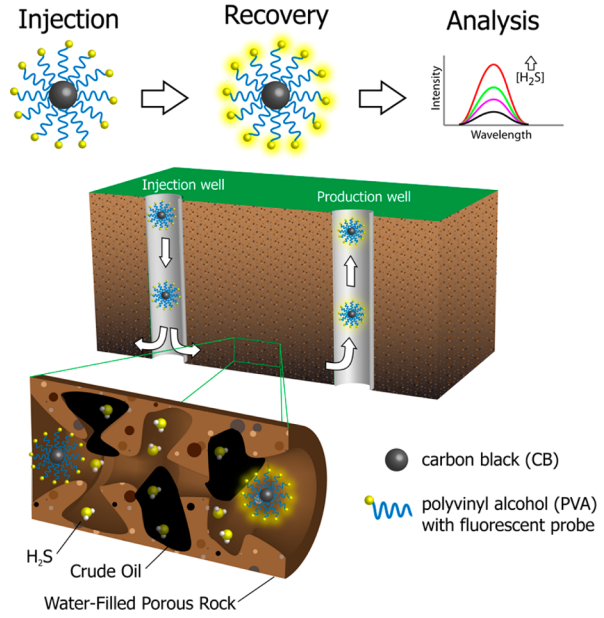

Figure 1. Schematic diagram of subsurface H_2S detection by nanoreporters bearing fluorescent probe molecules that are transported through rocks in the subsurface by pumping. The fluorescent properties of the functionalized NP would change based on the concentration of H_2S and the degree of functionalization of the NP. By the interrogation of the nanoreporter in the effluent at the production well, analysis of the fluorescence emission could give quantitative information regarding the H_2S content.

a scheme that outlines the use of a nanoreporter to detect subsurface H_2S. When the nanoreporter is pumped downhole, the H_2S-responsive nanoreporter would react with H_2S trapped in the water and oil deposits. The fluorescent properties of the functionalized NP would change based on the concentration of the H_2S and the degree of functionalization. By interrogation of the nanoreporter in the effluent at the production well, analysis of the fluorescence emission could give quantitative information regarding the downhole H_2S content.

RESULTS AND DISCUSSION

To prepare the thermally stable and mobile CB-based NPs, 15 nm CB (Cabot) was first functionalized with carboxylic groups by using the radical initiator 4,4′-azobis(4-cyanopentanoic acid) (ACPA) that produces a carboxyl group-functionalized CB.[17,18] Here 3.0 g of 15 nm carbon black (Cabot Monarch Lot # 1278105) was added to 100 mL of THF in a 250 mL round-bottom flask fixed with a stir bar and a rubber septum. The mixture was bath-sonicated (Cole-Parmer, 12 W, Model: 08849-00) for 3 h. 4,4′-Azobis(4-cyanopentanoic acid) (ACPA) (2.0 g, 7.0 mmol) was added to the flask and the reaction mixture was stirred at 65 to 70 °C for 24 h. At that point, a second portion of ACPA (2.0 g, 7.0 mmol) was added and the mixture was stirred for another 24 h. Finally, a third portion of ACPA (2.0 g, 7.0 mmol) was added with continued stirring for 24 h. After the mixture cooled to room temperature, it was filtered through a 0.45 μm PTFE membrane and the black solid was washed with THF (3×), ethanol (3×) and acetone (3×). The solid was dried at 60 °C under vacuum (100 Torr). 2000 molecular weight polyvinyl alcohol (PVA(2k)) was subsequently grafted onto the carboxyl-functionalized CB core by condensation of the hydroxyl groups of the PVA with the carboxyl groups through a *N,N*′-dicyclohexylcarbodiimide (DCC) coupling reaction. Unbound PVA was removed by dialysis of the reaction product against running deionized (DI) water. The PVA(2k) grafted CB (PVA(2k)-CB) was finally obtained. The detailed synthetic process is in the Supporting Information.

Figure 2A shows the attenuated total reflectance infrared (ATR-IR) spectra of the CB after the PVA(2k) modification.

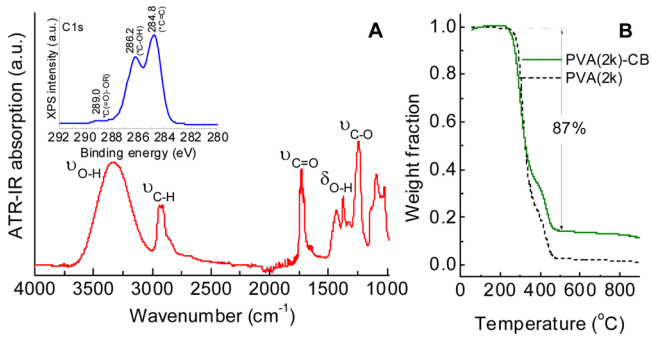

Figure 2. (A) ATR-IR spectra of the PVA(2k)-CB NPs, including an inset that is the high resolution C 1s XPS of the NPs. (B) TGA of the PVA(2k)-CB NPs and the PVA(2k) as a control group. Samples were pretreated at 120 °C for dehydration prior to being heated to 900 °C at a rate of 3 °C/min in argon.

The PVA(2k)-CB spectrum was observed to have two broad peaks centered at 3320 and 2920 cm^{-1} that correspond to the stretching modes of the O−H and C−H, respectively, on the PVA.[19] The peak at 1735 cm^{-1} was assigned to carbonyl vibrations of the ester groups on the PVA(2k)-CB NPs, which confirmed that the PVA was grafted through chemical functionalization to the CB surface instead of only being physisorbed.[17] Extended dialysis treatment (7 days) was assumed to have removed all noncovalently bound PVA. The adsorption band from 1000 to 1300 cm^{-1} was attributed to C−O−C and C−OH stretching due to ester, ether and alcohol moieties. High resolution X-ray photoelectron spectroscopy (XPS) was further used to analyze the surface chemical structures on the PVA(2k)-CB so as to corroborate the ATR-IR analysis. The C 1s XPS spectrum of the PVA(2k)-CB (Figure 2A, inset) showed two apparent peaks at 284.8 and 286.2 eV, which can be attributed to the sp^2 carbon on the carboxyl-

dx.doi.org/10.1021/am5009584 | ACS Appl. Mater. Interfaces 2014, 6, 7652−7658

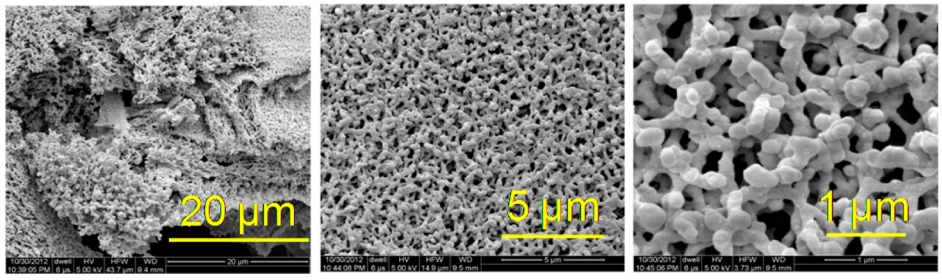

Figure 3. SEM images taken from the PVA(2k)-CB. The NPs originally dispersed in aqueous solution were concentrated, followed by being precipitated through the addition of acetone.

functionalized CB and the carbon attached to the OH group, respectively.[20] Also, a weak band ~289.0 eV can be assigned to the carbon in the ester moieties, further evidence that the PVA polymers were covalently attached to the CB surface. Because the polymer brushes are assumed to surround the CB core via the ester linkages and therefore create a thick protective shell, the corresponding XPS signal from the ester group was weakened. Thermogravimetric analysis (TGA) also provides evidence for the amount of the PVA on the CB cores (Figure 2B). The PVA(2k)-CB showed 87 wt % loss from 250 to 500 °C, which is reasonably attributed to the decomposition of the PVA(2k)-CB as compared to the profile of the starting polymer PVA(2k).

Figure 3 shows scanning electron microscopy (SEM) images of the PVA(2k)-CB. These NPs samples were prepared by precipitating the concentrated PVA(2k)-CB in 500 mL of acetone followed by filtration and drying of the filter cake under vacuum (~100 Torr) overnight at ambient temperature. Even though these NPs showed agglomeration due to the bridging effect between the polymers in the acetone, they still retained the spherical shape characteristic of carbon black.

A colloidal system can be stable if the repulsive forces that exist between the particles prevail over the attractive forces as the particles approach one another. The CB bearing carboxyl groups could be expected to have negative surface charges under neutral pH; therefore, the electrostatic repulsion between those charged NPs provides a stabilizing mechanism in the colloidal system. It is therefore possible for the carboxyl-functionalized CB to be dispersed in deionized water after sonication (Figure 4A). After 6 h without sonication, the carboxyl-functionalized CB particles precipitated as a result of insufficient electrostatic stabilization (Figure 4B). This assumption could be indirectly supported by dispersing the carboxyl-functionalized CB into a synthetic seawater solution (see the Supporting Information) because these charge-stabilized NPs are sensitive to addition of salt, in particular, high valency counterions.[21] When the electrolyte concentration increases, the corresponding Debye length of the colloidal system lessens, and the decay of the electrostatic stabilization rapidly causes the NPs to agglomerate (Figure 4C).[22] When the carboxyl-functionalized CB was further functionalized with PVA(2k), the colloidal system was stabilized via the steric repulsive force between the polymer brushes (Figure 4D). Unfortunately, the PVA(2k)-FCB did not remain well-dispersed and the solution became turbid as the temperature was elevated to 70 °C, the cloud point of the PVA(2k), above which aggregations of the NPs could be expected (Figure 4E).[23,24] Functionalization with longer chain stabilizing polymers, such as PVA(50k) and PVA(100k) with cloud points that are higher than that of the PVA(2k), the CB

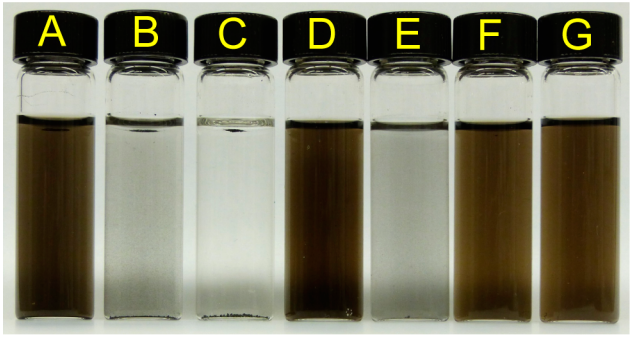

Figure 4. Photographs taken from (A) the carboxyl-functionalized CB dispersed in DI water after sonication. (B) After 6 h without sonication, the carboxyl-functionalized CB NPs precipitated from the suspension. (C) In spite of sonication, the carboxyl-functionalized CB NPs could not be dispersed in synthetic seawater. (D) After functionalization with the PVA(2k) polymer brushes, the PVA(2k)-CB NPs were stable in synthetic seawater without precipitation at room temperature. (E) When the temperature was elevated to 70 °C, the colloidal system became cloudy as the temperature reached the cloud point of the PVA(2k) and the particles precipitated. Both (F) PVA(50k)-CB and (G) PVA(100k-CB were stable colloidal systems in synthetic seawater at 100 °C.

colloidal system remained stable in synthetic seawater at high temperature (100 °C, Figure 4F,G).

To quantify particle size at different temperatures, dynamic light scattering (DLS) was applied to observe the changes in particle sizes of the PVA-CB over a temperature range from 25 to 70 °C (Figure 5). All NPs were purified by filtration through a 0.22 μm Millipore Express PES membrane filter, followed by dispersion in the synthetic seawater prior to the light scattering measurements. The PVA-CB, hydrodynamic radii were all similar at 25 °C. However, the particle size of the PVA(2k)-CB and the PVA(10k)-CB drastically increased with elevated temperature as expected by the Stokes-Einstein equation; their particle sizes increased to 530 and 500 nm, respectively, at 70 °C. Compared to PVA(2k) and PVA(10k), PVA(50k) and PVA(100k) provided CB with sufficient steric repulsion so that the functionalized CB NPs were stable with no apparent agglomeration. The instability at lower molecular weights can be attributed to the thermal-induced loss of the water molecules surrounding the smaller PVA polymer chain, resulting in aggregation.

To evaluate the PVA-CB NPs under more challenging conditions, the NPs were pumped through sandstone, a natural rock that is commonly found in oilfields, to mimic an oilfield environment.[25] The ground sandstone (89−251 μm) was packed into a glass column. The corresponding pore volume (PV) of the sandstone-packed column could be calculated by

dx.doi.org/10.1021/am5009584 | ACS Appl. Mater. Interfaces 2014, 6, 7652−7658

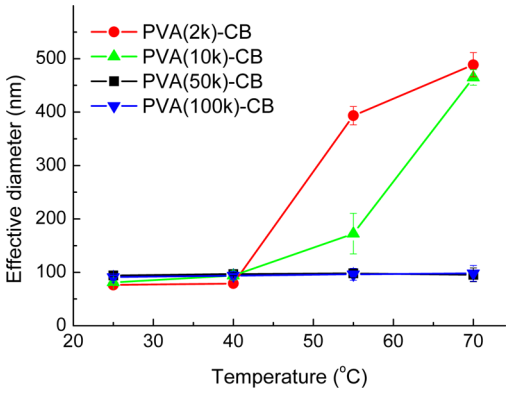

Figure 5. Temperature-dependent DLS measurements for the CB NPs after being modified with a variety of PVA molecular weights. All of the PVA-CB NPs were purified by filtration through a 0.22 μm membrane filter, followed by dispersion in seawater before the DLS measurement. The system temperature was elevated from 25 to 70 °C at a heating rate of ~5 °C/min.

saturating the column with liquid. The concentration of the PVA-CB NPs in the effluent (C) relative to the initial concentration in the influent (C_0) was measured by its UV absorbance at 232 nm and the C/C_0 ratio was then used to evaluate the transport efficiency for the PVA-CB NPs. Figure 6

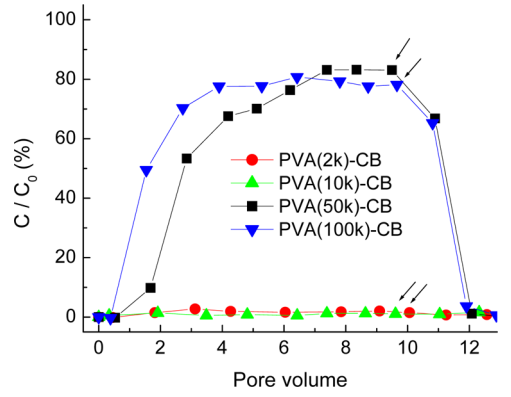

Figure 6. Breakthrough studies for PVA-CB NPs in sandstone-packed columns. Synthetic seawater prepared to be equivalent to seawater was chosen as the carrier solution for the NPs. The temperature remained at 70 °C during the injection process and transport, with a flow rate of 8 mL/h and a linear velocity of 9.3 m/d. The percentage of PVA-CB NPs in the effluent (C) relative to the influent (C_0) was determined by UV spectroscopy. The arrows indicate when the flow was switched from the PVA-CB NPs to pure synthetic seawater.

shows the relative breakthrough performances of the PVA-CB modified by different molecular weight PVA, while they were pumped through the sandstone-packed column at 70 °C. The PVA(50k)-CB and the PVA(100k)-CB yielded asymmetrical breakthrough curves that reached ~80% in 7 PV; PVA(2k)-CB and PVA(10k)-CB did not smoothly flow through but blocked the column, finally resulting in limited breakthrough efficiencies. These outcomes were in agreement with the DLS results. According to the data, the PVA(50k)-CB and the PVA(100k)-CB NPs would be the better transporter candidates for nanoreporter downhole exploration because of their thermal stabilities and efficient mobilities under critical environmental conditions.

The PVA-CB NPs were next functionalized to monitor H_2S concentration downhole. This was done using molecules designed for selective imaging of H_2S in living cells, a probe reported to afford highly sensitive and selective monitoring of H_2S by a turn-on fluorescence signal enhancement.[26] Inspired by the structure of the new probe, a naphthalimide-based molecule was selected as a model compound to functionalize the PVA(50k)-CB. The combination was anticipated to have the potential for monitoring H_2S in the subsurface.

Commercially available 3-nitro-1,8-naphthalic anhydride (**1**, Scheme 1A) was chosen as the starting material. It could be converted to a naphthalimide by the addition of 6-aminocaproic acid. The extended aliphatic moiety in **2** was designed to covalently bond to the PVA chains of the PVA-CB via ester bond linkages. The naphthalimide bearing a 3-nitro electron-withdrawing group (EWG) was nonfluorescent because of the EWGs from the imide and the 3-nitro resulting in a "pull−pull" configuration, making the intramolecular charge transfer (ICT) process forbidden.[27,28] Upon conversion of the nitro group to a nitroamine by catalytic reduction, an electron-donating group (EDG), the ICT process would be restored, leading to a large fluorescent enhancement through the "push−pull" configuration.[26] The nitro group was converted to a hydroxylamine, **3**, a relatively stable intermediate that is easily reduced by H_2S. Scheme 1A shows the synthesis of the probe molecule **3** and how the PVA-CB was functionalized with the fluorescent probe (FP) to produce the nanoreporter FP-PVA-CB (Scheme 1B).

The nanoreporter FP-PVA(50k)-CB and a series of given concentrations of $Na_2S_{(aq)}$ (commonly used as H_2S precursor at these concentrations) were separately dissolved in seawater before the solutions were simultaneously injected into a sandstone-packed column by an automatic injection system (Scheme 2). The pump rate was controlled at 0.6 mL/h for each syringe pump, for the reduction reaction to occur in the column. The recovered solution was subsequently monitored by fluorescence spectroscopy, and the change in the fluorescence after each breakthrough study was recorded in Figure 7.

Figure 7 illustrates that the fluorescence change when 50 μM of the FP-PVA(50k)-CB was reacted with a series of concentrations of $H_2S_{(aq)}$ from 0 to 170 μM in the sandstone-packed column. Na_2S is commonly used as a replacement for the H_2S because both form HS^- in solution. Indeed, fluorescence enhancement was observed when treating the nanoreporter with the $H_2S_{(aq)}$. The change in fluorescence intensity was found to be in direct proportion to the introduced concentration of the $H_2S_{(aq)}$, reaching an 11-fold enhancement at ~70 μM of the H_2S concentration, which is close to the higher-end H_2S concentration in sour oilfields. While the higher concentration of the H_2S (170 μM) was added to react with the nanoreporter, the enhancement of the fluorescence intensity plateaued. This suggests that the probe molecules on the nanoreporters were fully reduced by the H_2S. The overall reduction of the hydroxyl amine to the amine moiety is summarized in Scheme 3.

Finally, a new column that was packed with Kuwaiti oilfield dolomite and Berea sandstone was used to replace the original sandstone-packed column in order to better simulate the actual oilfield environment. As Figure S5 (left) (Supporting Information) shows, the FP-PVA(50k)-CB not only had >95% breakthrough efficiency in 6 PVs but also exhibited good response to the H_2S (Figure S5 (right) (Supporting Information)). The fluorescent enhancement was comparable

dx.doi.org/10.1021/am5009584 | ACS Appl. Mater. Interfaces 2014, 6, 7652−7658

Scheme 1. (A) Synthetic Route to the H_2S-Responsive Fluorescent Probe, 3, and (B) Fluorescent Probes Condensed with PVA-CB to Produce a Nanoreporter (FP-PVA-CB) Purified by Dialysis[a]

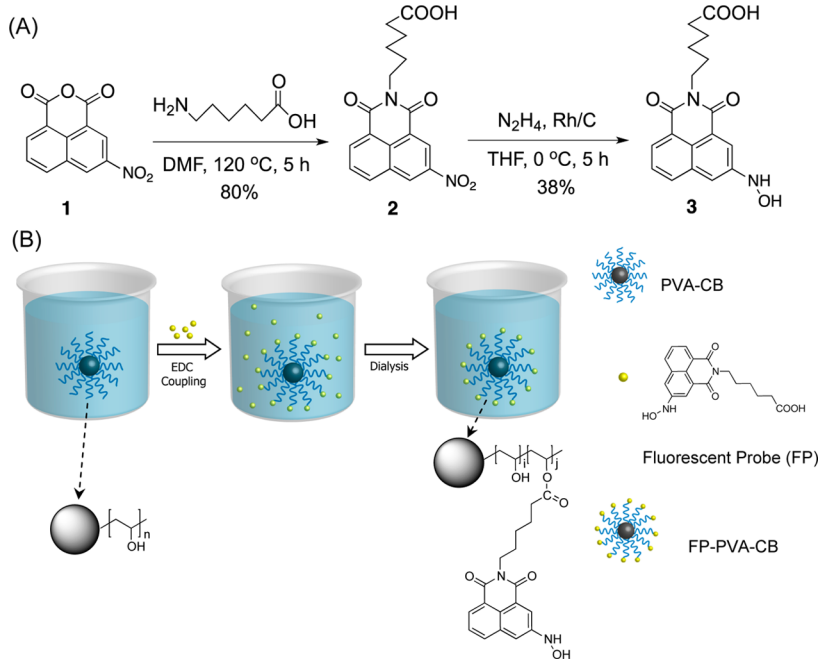

[a]In panel B, the picture only shows the FP at the end of the polymer chains; however, they are functionalized throughout many of the repeat units.

Scheme 2. Configuration of the Apparatus for the Laboratory Detection and Quantitative Analysis of Hydrogen Sulfide Content in Simulated Downhole Rocks[a]

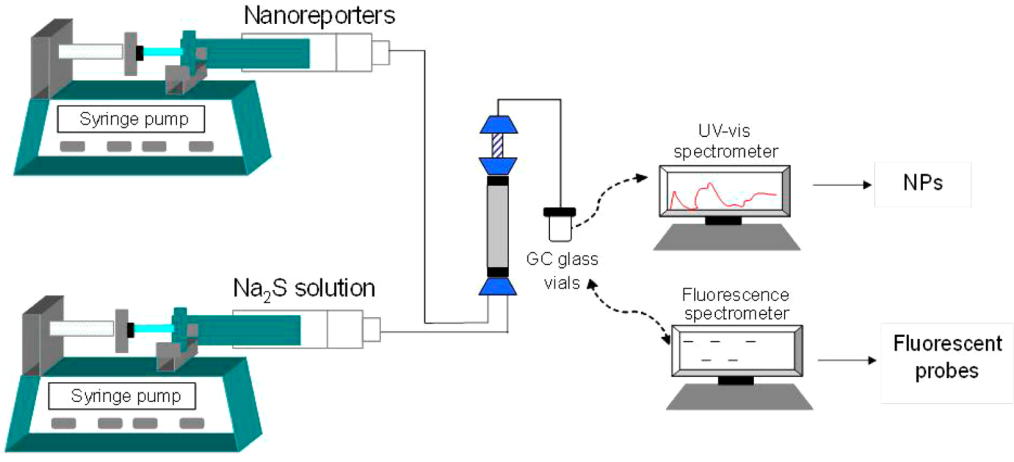

[a]The nanoreporter FP-PVA(50k)-CB and the Na_2S (H_2S precursor at these concentrations) were diluted into seawater before simultaneous injection into a sandstone-packed column at a pump rate = 0.6 mL/h. The concentration of the nanoreporter was measured by the UV−vis absorbance at 412 nm (ε = 33 832 M^{-1} cm^{-1}). 50 μM of the FP-PVA(50k)-CB and various concentrations of $Na_2S_{(aq)}$ (from 0 to 170 μM) were recovered and the amount of H_2S monitored through fluorescence spectroscopy.

to that from the nanoreporter in the sandstone-backed column containing the same H_2S concentration (Figure 7B), suggesting that the PVA-coated nanoreporter is not trapped by crude oil. Additionally, the change in fluorescence enhancement depends upon the concentration of H_2S in the column and not the type of rock formation.

CONCLUSION

In conclusion, PVA-CB NPs were synthesized and they exhibited efficient mobility as well as thermal stability under simulated downhole environments. The PVA-CB NP was subsequently functionalized with a H_2S-sensitive probe molecule to show H_2S detection in a simulated subsurface system. By taking advantage of the reducing efficiency of H_2S, the ICT of π-conjugate push−pull properties of the probe molecule resulted in fluorescence enhancement. The FP-PVA-CB nanoreporter gave quantitative information on the H_2S content based upon fluorescence enhancement. This was demonstrated in both laboratory rock columns and in actual oilfield rock containing natural oil, underscoring the efficacy of this approach.

dx.doi.org/10.1021/am5009584 | ACS Appl. Mater. Interfaces 2014, 6, 7652−7658

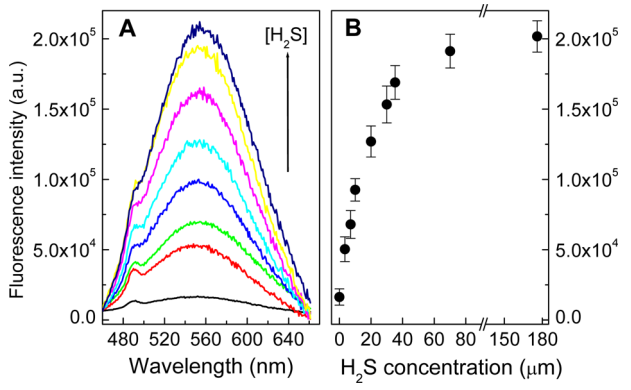

Figure 7. (A) Fluorescence spectra of the 50 μM FP-PVA(50k)-CB nanoreporter after pumping through the sandstone-packed columns containing different concentrations of $H_2S_{(aq)}$. The fluorescence experiment was conducted at 25 °C with an excitation λ_{ex} = 420 nm. (B) correlation of the H_2S concentration vs the fluorescence intensity taken at λ_{em} = 550 nm.

Scheme 3. Change of the Functional Groups on the Nanoreporter during the H_2S Detection Process

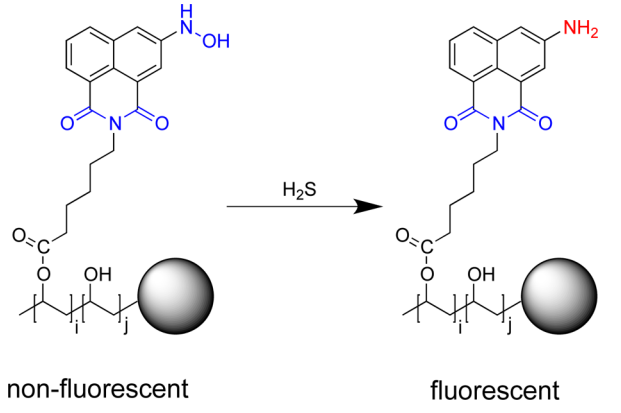

■ ASSOCIATED CONTENT

Supporting Information

Synthesis of carboxyl-functionalized CB, synthesis of PVA-grafted carboxyl-functionalized CB (PVA-CB), preparation of the probe molecule 6-(5-(hydroxyamino)-1,3-dioxo-1H-benzo-[de]isoquinolin-2(3H)-yl)hexanoic acid (compound **3**), preparation of the probe molecule-PVA-CB (FP-PVA-CB), preparation of seawater, ATR-IR spectra for the starting material **1**, intermediate **2**, and product **3**, electrospray ionization mass spectra for compounds **2** and **3**, ^{1}H NMR (500 MHz, DMSO-d_6, 293 K) of compound **2**, ^{1}H NMR (500 MHz, DMSO-d_6, 293 K) of compound **3**, and breakthrough study for the FP-PVA(50k)-CB nanoreporter. This material is available free of charge via the Internet at http://pubs.acs.org.

■ AUTHOR INFORMATION

Corresponding Authors

*J. M. Tour. E-mail: tour@rice.edu.
*M. B. Tomson. E-mail: mtomson@rice.edu.
*M. S. Wong. E-mail: mswong@rice.edu.

Author Contributions

#Authors contributed equally.

Notes

The authors declare no competing financial interest.

■ ACKNOWLEDGMENTS

This work was supported by the Advanced Energy Consortium: http://www.beg.utexas.edu/aec/. Member companies include BP America Inc., BG Group, Petrobras, Schlumberger, Statoil, Shell, and Total. The authors also thank Mr. Varun Gangoli for assistance with the dynamic light scattering (DLS) measurement.

■ REFERENCES

(1) "PubChem Public Chemical Database" National Center for Biotechnology Information. http://pubchem.ncbi.nlm.nih.gov/summary/summary.cgi?cid=402 (accessed 12/4/13).
(2) "Toxicological Profile For Hydrogen Sulfide" Agency for Toxic Substances and Disease Registry. http://www.atsdr.cdc.gov/ToxProfiles/tp.asp?id=389&tid=67 (accessed 12/4/13).
(3) Lewis, R. J. *Sax's Dangerous Properties of Industrial Materials*, 9th Ed.; Van Nostrand Reinhold: New York, NY, 1996.
(4) Li, L.; Bhatia, M.; Moore, P. K. Hydrogen Sulphide – a Novel Mediator of Inflammation? *Curr. Opin. Pharmacol.* **2006**, *6*, 125–129.
(5) Selley, R. C. *Elements of Petroleum Geology*, 2nd Ed.; Academic Press: San Diego, CA, 1998.
(6) "Processing Natural Gas" National Gas. http://www.naturalgas.org/naturalgas/processing_ng.asp (accessed 12/3/13).
(7) "Heavy Sour Crude Oil, A Challenge For Refiners" http://www.commodity-trading-today.com/sour-crude-oil.html (accessed 12/4/13).
(8) Wang, Y.; Li, Y.; Fortner, J. D.; Hughes, J. B.; Abriola, L. M.; Pennell, K. D. Transport and Retention of Nanoscale C_{60} Aggregates in Water-Saturated Porous Media. *Environ. Sci. Technol.* **2008**, *42*, 3588–3594.
(9) Li, Y.; Wang, Y.; Pennell, K. D.; Abriola, L. M. Investigation of the Transport and Deposition of Fullerene (C_{60}) Nanoparticles in Quartz Sands under Varying Flow Conditions. *Environ. Sci. Technol.* **2008**, *42*, 7174–7180.
(10) Lecoanet, H. F.; Bottero, J. Y.; Wiesner, M. R. Laboratory Assessment of the Mobility of Nanomaterials in Porous Media. *Environ. Sci. Technol.* **2004**, *38*, 5164–5169.
(11) Jaisi, D. P.; Elimelech, M. Single-Walled Carbon Nanotubes Exhibit Limited Transport in Soil Columns. *Environ. Sci. Technol.* **2009**, *43*, 9161–9166.
(12) Wang, P.; Shi, Q.; Liang, H.; Steuerman, D. W.; Stucky, G. D.; Keller, A. A. Enhanced Environmental Mobility of Carbon Nanotubes in the Presence of Humic Acid and Their Removal from Aqueous Solution. *Small* **2008**, *4*, 2166–2170.
(13) Lenhart, J. J.; Saiers, J. E. Transport of Silica Colloids Through Unsaturated Porous Media: Experimental Results and Model Comparisons. *Environ. Sci. Technol.* **2002**, *36*, 769–777.
(14) He, F.; Zhang, M.; Qian, T.; Zhao, D. Transport of Carboxymethyl Cellulose Stabilized Iron Nanoparticles in Porous Media: Column Experiments and Modeling. *J. Colloid Interface Sci.* **2009**, *334*, 96–102.
(15) Saleh, N.; Sirk, K.; Liu, Y.; Phenrat, T.; Dufour, B.; Matyjaszewski, K.; Tilton, R. D.; Lowry, G. V. Surface Modifications Enhance Nanoiron Transport and NAPL Targeting in Saturated Porous Media. *Environ. Eng. Sci.* **2007**, *24*, 45–57.
(16) Berlin, J. M.; Yu, J.; Lu, W.; Walsh, E. E.; Zhang, L.; Zhang, P.; Chen, W.; Kan, A. T.; Wong, M. S.; Tomson, M. B.; Tour, J. M. Engineered Nanoparticles for Hydrocarbon Detection in Oil-Field Rocks. *Energy Environ. Sci.* **2011**, *4*, 505–509.
(17) Hwang, C. C.; Wang, L.; Lu, W.; Ruan, G.; Kini, G. C.; Xiang, C.; Samuel, E. L. G.; Shi, W.; Kan, A. T.; Wong, M. S.; Tomson, M. B.; Tour, J. M. Highly Stable Carbon Nanoparticles Designed for Downhole Hydrocarbon Detection. *Energy Environ. Sci.* **2012**, *5*, 8304–8309.
(18) Chen, J.; Tsubokawa, N. Novel Gas Sensor from Polymer-Grafted Carbon Black: Vapor Rresponse of Electric Resistance of Conducting Composites Prepared from Poly(Ethylene-*block*-Ethylene Oxide)-grafted carbon black. *J. Appl. Polym. Sci.* **2000**, *77*, 2437–2447.

(19) Shen, C. C.; Joseph, J.; Lin, Y. C.; Lin, S. H.; Lin, C. W.; Hwang, B. J. Modifying Microphase Separation of PVA Based Membranes for Improving Proton/Methanol Selectivity. *Desalination* **2008**, *233*, 82−87.
(20) Marcano, D. C.; Kosynkin, D. V.; Berlin, J. M.; Sinitskii, A.; Sun, Z.; Slesarev, A.; Alemany, L. B.; Lu, W.; Tour, J. M. Improved Synthesis of Graphene Oxide. *ACS Nano* **2010**, *4*, 4806−4814.
(21) Napper, D. H. *Polymeric Stabilization of Colloidal Dispersions*; Academic Press: New York, 1983.
(22) Cosgrove, T. *Colloid Science: Principles, methods and applications*, 2nd Ed.; John Wiley & Sons, Ltd.: New York, 2010.
(23) Derjaguin, B. V.; Landau, L. Theory of the Stability of Strongly Charged Lyophobic Sols and of the Adhesion of Strongly Charged Particles in Solution of Electrolytes. *Acta Physicochim.* **1941**, *14*, 633−662.
(24) Verway, E. J.; Overbeek, J. T. G. *Theory of the Stability of Lyophobic Colloids*; Elsevier: Amsterdam, 1948.
(25) Folk, R. L. *Petrology of Sedimentary Rocks*; Hemphill Publishing Company: Austin, Texas, 1981.
(26) Xuan, W.; Pan, R.; Cao, Y.; Liu, K.; Wang, W. A Fluorescent Probe Capable of Detecting H_2S at Submicromolar Concentrations in Cells. *Chem. Commun.* **2012**, *48*, 10669−10671.
(27) Kucheryavy, P.; Li, G.; Vyas, S.; Hadad, C.; Glusac, K. D. Electronic Properties of 4-Substituted Naphthalimides. *J. Phys. Chem. A* **2009**, *113*, 6453−6461.
(28) Montoya, L. A.; Pluth, M. Selective Turn-on Fluorescent Probes for Imaging Hydrogen Sulfide in Living Cells. *Chem. Commun.* **2012**, *48*, 4767−4769.